

Article

Corrosion Effect of Biodiesel-Diesel Blend on Different Metals/Alloy as Automotive Components Materials

Ancaelena Eliza Sterpu , Bianca Georgiana Simedrea, Timur Vasile Chis and Olga Valerica Săpunaru * 

Department of Chemistry and Chemical Engineering, Ovidius University of Constanta, 124 Mamaia Blvd, 900527 Constanta, Romania; asterpu@univ-ovidius.ro (A.E.S.); simedrea.bianca@yahoo.com (B.G.S.); timur.chis@gmail.com (T.V.C.)

* Correspondence: olga.sapunaru@365.univ-ovidius.ro; Tel.: +40-762-520-001

Abstract: Biodiesel has emerged as a progressively widespread and significant alternative to traditional diesel fuel within the transportation sector. Despite its growing popularity, the issue of corrosive tendencies upon interaction with both moving and static components of diesel engines and fuel systems poses a serious concern. This research endeavors to assess the corrosion characteristics of materials commonly found in automotive fuel systems when exposed to various blends of rapeseed oil biodiesel and diesel. The study involved static immersion tests, lasting 3360 h at room temperature, using B0, B20, B40, B60, B80, and B100 fuels. Copper, brass, aluminum, zinc, and stainless steel plate samples were subjected to these tests. The evaluation at the conclusion of the study included weight loss measurements, corrosion rate calculations, and observation of changes in the exposed metal surfaces. Surface morphology was scrutinized using a Bresser LCD MICRO 5MP digital microscope. Additionally, the total acid number (TAN) was employed to assess alterations in fuel acidity before and after the immersion tests.

Keywords: rapeseed oil biodiesel; corrosion; metals/alloys; static immersion test; corrosion rate



Citation: Sterpu, A.E.; Simedrea, B.G.; Chis, T.V.; Săpunaru, O.V. Corrosion Effect of Biodiesel-Diesel Blend on Different Metals/Alloy as Automotive Components Materials. *Fuels* **2024**, *5*, 17–32. <https://doi.org/10.3390/fuels5010002>

Academic Editor: Javier Ereña

Received: 28 November 2023

Revised: 23 December 2023

Accepted: 9 January 2024

Published: 15 January 2024



Copyright: © 2024 by the authors. Licensee MDPI, Basel, Switzerland. This article is an open access article distributed under the terms and conditions of the Creative Commons Attribution (CC BY) license (<https://creativecommons.org/licenses/by/4.0/>).

1. Introduction

Biodiesel, made from renewable sources like vegetable oils and animal fats, is commonly mixed with regular diesel to create more environmentally friendly fuel options. Among the various biodiesel formulations, rapeseed oil biodiesel has gained significant attention due to its favorable characteristics, such as high energy content, low sulfur content, and potential for reduced greenhouse gas emissions. While the environmental benefits are evident, the interaction between biodiesel-diesel blends and automotive materials deserves meticulous scrutiny. Different metals and alloys used in the construction of automotive components may respond differently to the corrosive environment created using these biofuels. Parts like fuel pumps, gaskets, fuel injectors, filters, fuel liners, bearings, pistons, and piston rings are exposed to biodiesel, requiring careful consideration [1–7]. In recent research [8], palm biodiesel has emerged as the most commonly utilized biodiesel due to its favorable fuel properties. Among the metals frequently studied in relation to this biodiesel are aluminum, stainless steel, mild steel (also known as low carbon steel), cast iron, copper, and copper-based alloys like bronze.

As highlighted in several studies [9], a significant portion of engine parts and fuel system components are fabricated from metals and alloys such as aluminum, copper, iron, and stainless steel, all of which are prone to corrosion. Specifically, components made from copper alloys, including fuel pumps, bearings, and bushings, are notably affected by the type of fuel they encounter [10]. Recommendations suggest that materials like copper, aluminum, zinc, brass, and bronze do not pair well with biodiesel [11]. In compact diesel engines, aluminum or its alloys are used for parts like pistons, cylinder heads, and engine blocks. Meanwhile, copper and its derivatives are chosen for fuel pump elements and

injector parts, and stainless steel is preferred for components like fuel filters, valve bodies, and pump rings [12]. To assess and examine the corrosion susceptibility of these metals and alloys, the simplest method involves observing changes in the color of biodiesel. However, other methodologies, such as the static immersion test (SIT) under varying temperature conditions, should also be taken into consideration [13]. Upon completion of the SIT, the corrosion behavior of metals exposed to biodiesel is evaluated by determining the corrosion rate (CR) expressed in millimeters per year (mm/year) [14].

Furthermore, both conventional and modern equipment can be employed for the examination of microstructural changes on metal surfaces. In a conducted study [15], the corrosive behavior of biodiesel in a diesel engine was explored with a focus on injector and burner filter components. The injector was crafted from high chrome stainless steel, while copper and copper-based alloys were utilized in the burner filter components. The study revealed an escalation in copper content in biodiesel fuel, rising from 0.1 to 21 ppm after a 2 h test. Notably, corrosion, including pitting, was observed on the bronze filter after 10 h of using preheated biodiesel at 70 °C; however, no signs of corrosion were detected on the injector.

In another work [16], researchers examined the corrosion characteristics of mild steel when submerged in various fuels: B0 (100% diesel), B50 (50% palm biodiesel and 50% diesel), and B100 (100% palm biodiesel), all conducted at room temperature for a duration of 1200 h.

Another study [17] examines the corrosion characteristics of five metals commonly employed in automotive part production when subjected to pure palm biodiesel (B100) and palm biodiesel combined with typical acidic components present in biodiesel. Samples of AISI-SAE 1005 carbon steel, AISI-SAE 304 stainless steel, tin, aluminum, and copper underwent exposure at a temperature of 45 °C over a 12-month period. Notably, the most pronounced corrosion rates were observed in copper samples fully immersed in a blend of B100 with acetic acid and in carbon steel samples exposed to a blend of B100 with oleic acid.

In a study by Hu et al. [18], an assessment was made on the corrosion characteristics of different metals such as copper, mild carbon steel, stainless steel, and aluminum when exposed to biodiesel in contrast to pure diesel. Following a 60 h immersion at 43 °C, it was observed that the corrosion rates in biodiesel surpassed those in diesel. Additionally, both copper and mild carbon steel exhibited notably higher corrosion rates compared to aluminum and stainless steel.

Geller et al. [19] and Aquino et al. [20] both presented findings that align with the susceptibility of copper and copper-based alloys, like brass, to pitting corrosion, as demonstrated via weight loss experiments. Meanwhile, Haseeb et al. [12] investigated the impact of palm oil biodiesel on copper and leaded bronze corrosion at room temperature across B0, B50, and B100 blends for a duration of 2640 h. Their results indicated corrosion rates of 0.042 mpy for copper and 0.018 mpy for bronze in the B100 blend.

In their research, Fazal et al. [21] focused on assessing the sustainability of palm biodiesel treated with additives when in contact with copper-based materials, including copper, leaded bronze, and phosphorous bronze. They conducted a static immersion test at a room temperature range of 25 °C to 27 °C for a duration of 2160 h. They examined two variants of the biodiesel: pure 100% palm biodiesel and palm biodiesel enriched with additives like tert-butylamine, benzotriazole, propyl gallate, pyrogallol, and butylated hydroxytoluene at a concentration of 500 ppm. Upon completing the experiment, they assessed the corrosion rate of these metals using weight loss measurements.

In a recent study [22], the authors examined the compatibility and corrosion tendencies of carbon steel, stainless steel, aluminum, and copper when exposed to blends of biodiesel made from soybean oil, beef tallow, and swine lard mixed with petrodiesel. They conducted static immersion tests, including total, partial, and crevice exposures, along with vapor phase exposure for a duration of 2160 h at a temperature of 50 °C. As a result, most materials

exhibited reduced corrosion rates, except for copper, which displayed unconventional corrosion behavior, indicating a noticeable tendency toward decreased corrosion rates.

Thangarasu et al. [23] investigated the tribo-corrosion and engine characteristics of Aegle Marmelos Correa biodiesel and its diesel blends on direct injection diesel engines and concluded that B100 is the ideal blend that can perform efficiently and be a sustainable energy source for diesel engines.

In a previous work [24], the corrosion behavior of biodiesel produced from sunflower, rapeseed, and corn oil on carbon steel plates was estimated during a static immersion test for 1176 h at room temperature. The results indicate that the corrosion rate of carbon steel was 0.00076 mm/year after immersion in biodiesel from rapeseed oil.

Problem Statement

The focus of the present study is to investigate the corrosion behavior of some materials commonly encountered in automotive fuel systems when exposed to different blends of rapeseed oil biodiesel and diesel fuel. Static immersion tests were conducted at room temperature for 20 weeks (3360 h), focusing on copper, brass, aluminum, zinc, and stainless steel plate samples. The biodiesel-diesel blends under investigation include B0 (100% diesel), B20 (20%biodiesel + 80% diesel), B40 (40%biodiesel + 60% diesel), B60 (60%biodiesel + 40% diesel), B80 (80%biodiesel + 20% diesel) and B100 (100% biodiesel).

The surface morphology of the plate samples is scrutinized using a Bresser LCD MICRO 5MP digital microscope (Rhede, Germany) with a 10× magnification level to provide a comprehensive understanding of the corrosion process.

The investigation not only aims to unravel the corrosion behavior using weight loss measurements and examination of the exposed metal surfaces but also evaluates changes in fuel acidity using the Total Acid Number (TAN) both before and after the immersion tests. The Total Acid Number (TAN) is an important parameter in assessing the corrosion behavior of metals in biodiesel-diesel blends.

TAN is a measure of the acidity of a fuel, indicating the presence of acidic compounds. In biodiesel, the acids are primarily free fatty acids (FFAs) resulting from the hydrolysis of triglycerides. The TAN is expressed as the amount of potassium hydroxide (KOH) in milligrams required to neutralize one gram of the sample. A higher TAN value indicates a higher acidity level [25]. Corrosion in metal components can occur when acidic compounds come into contact with metals, leading to the formation of corrosive products. The TAN is, therefore, a key indicator of the potential corrosiveness of biodiesel and biodiesel-diesel blends. Elevated TAN values can accelerate corrosion and adversely affect the durability and performance of engine and fuel system components. The corrosion process involves the interaction of acids with metal surfaces, promoting the formation of oxides and other corrosion products. This can result in the degradation of fuel system components, including fuel tanks, pipelines, and engine parts. Common metals affected by biodiesel-induced corrosion include aluminum, copper, and zinc [26].

The results obtained from this research aim to enhance our understanding of biodiesel's impact on the corrosion of automotive components and contribute valuable information for the ongoing development and implementation of biodiesel blends in the automotive industry.

2. Materials and Methods

2.1. Materials

Biodiesel from rapeseed oil (B100) and diesel fuel (B0) used in this work was supplied by a Crude oil refinery from Romania. The physical and chemical analysis reports of both biodiesel and diesel fuel provided by the supplier are summarized in Tables 1 and 2.

Table 1. Analysis report of biodiesel from rapeseed oil for diesel engine types.

Analysis	Result	Conditions	Methods
Ester content, %	97.9	Min 96.5	[27]
C 18.3—Methyl Linoleate, %	4	-	[27]
Saturated fatty acids esters content, %	16		[27]
Iodine value, g/100g	80	Max. 120	[28]
Appearance at 15 degrees	Clear	Clear	Visual
Density at 15 °C, kg/m ³	883.1	880–900	[29]
Cinematic viscosity at 40 °C, mm ² /s	4.50	3.50–5.00	[30]
Water content, %	0.023	Max. 0.050	[31]
Methanol, %	0.10	Max. 0.20	[32]
Flash point, °C	123	Min. 101	[33]
Sulfur, mg/kg	<10.0	Max. 10.0	[34]
Oxidation stability at 110 °C, h	8.4	Min. 8.0	[35]
Acid value, mg KOH/g	0.28	Max. 0.50	[36]
Monoglyceride, %	0.63	Max. 0.70	[37]
Diglyceride, %	0.13	Max. 0.20	[37]
Triglyceride, %	0.03	Max. 0.20	[37]
Free glycerol, %	0.02	Max. 0.02	[37]
Total glycerol, %	0.21	Max. 0.25	[37]
Cold filter plugging point, °C	−11	Max. −10	[38]
Cloud point, °C	−3	Max. −3	[39]
Total contamination, mg/kg	17	Max. 24	[40]

Table 2. The physical and chemical properties of diesel fuel.

Analysis	Result	Conditions	Methods
Density at 15 °C, g/cm ³	0.827	0.82–0.845	[41]
ASTM Color, ASTM unit.	0.5	Max. 2.0	[42]
Flash point PENSKEY MARTENS, °C	59	Min. 55	[43]
Sulfur, mg/kg	9.0	Max. 10.0	[44]
Cinematic viscosity at 40 °C, mm ² /s	2.60	2.00–4.50	[30]
Corrosion on copper (3 h/100 °C)	1a	1 class	[45]
Carbon residue, %	0.025	Max. 0.3	[46]
Ash oxide, %	0.004	Max. 0.01	[47]
Cetane index,	54.5	Min. 46	[48]
Cloud point, °C	−4		[49]
Cold filter plugging point, °C	−17	Max. −15	[50]
Water content KF, mg/kg	100	Max. 200	[51]
Distillation at 250 °C, % vol.	39	Max. 65	[52]
Distillation at 350 °C, % vol.	93	Min. 85	[52]
Distillation at 95% vol., °C	355	Max. 360	[52]
FAME, % vol.	0	Max. 7	[53]
Density at 15 °C in air, g/cm ³	0.8259	-	[41,54]
Appearance	Clear	Clear	Visual

2.2. Corrosion Experiment

A total of 30 metal plates were prepared to conduct the immersion test experiments. These included six plates, each made of copper, brass (80% Cu), aluminum, zinc, and stainless steel (18% Cr, 10% Ni, 0.05% C). Every set of 6 plates of the same metal or alloy was immersed in 6 different fuel concentrations (B0, B20, B40, B60, B80, and B100). All 30 metal plates were completely immersed in 30 glass test tubes sealed tightly with transparent plastic film and kept in a dark place.

Before immersion, the surface of each metal plate was treated as follows: polished with emery, then cleaned and degreased with acetone at room temperature, followed by washing in deionized water. Only after drying were the coupons immersed in fuel. Before and after immersion of the plates into different test fuels, weight was measured using a balance with four decimal accuracy. The initial weight (m_1) of each metal sample was then measured. All

metal plates were placed in sets of six test tubes, each set containing blends of biodiesel-diesel in the proportions B0, B20, B40, B60, B80, and B100 at room temperature for 20 weeks (3360 h).

Every 2 weeks (336 h), during the immersion test, the metal plates were taken out, degreased with acetone, and washed with deionized water to remove impurities on the metals' surfaces. The cleaned metals were dried, and their weights were measured (m_2).

At the end of the test, corrosion behavior was investigated by measurement of corrosion rate and changes in surface morphology. The degree of corrosion was determined by measuring the corrosion rate (mm/year) according to Equation (1) [18]:

$$CR = \frac{(m_1 - m_2) \times 24 \times 365}{\rho TS \times 1000} \quad (1)$$

where m_1 is the weight before corrosion, g; m_2 is the weight after corrosion, g; CR is the corrosion rate, mm/year; ρ is the metal density, g/cm³; T is the corrosion time, h; and S are metal area of corrosion which was from the exposed metal plates, m². The length, width and height of metal blocks were measured using a micrometer.

2.3. Corrosion Analysis

During the immersion test, the metals were inserted completely into the biodiesel-diesel blends at room temperature (20–25 °C).

Corrosion products on metal surfaces exposed to each biodiesel-diesel blend were examined using a Bresser LCD MICRO 5MP digital microscope with a 10× magnification level. This apparatus incorporates a digital camera and an LCD screen directly into the microscope, allowing users to view specimens without the need for an external monitor or computer.

Before and after the immersion test, the fuels were analyzed by measuring the total acid number (TAN) in order to investigate the changes in acidity. The measurement of TAN for all biodiesel-diesel blends followed the [36].

3. Results

Changes in Mass and Appearance of Metalsplates

For each copper, brass, aluminum, zinc, and stainless steel plate, immersion tests were conducted in B0, B20, B40, B60, B80, and B100 at room temperature for 20 weeks (3360 h). All experimental values resulted from a single sample for each condition. The weight loss values (in %) of each metal plate measured every two weeks (336 h) were calculated with Equation (2). and presented in Figures 1–5. The corrosion rate of each metal: copper, brass, aluminum, zinc, and stainless steel after 3360 h of immersion in all six biodiesel-diesel blends (B0, B20, B40, B60, B80, and B100) at room temperature, are presented in Figure 6.

$$wl (\%) = \frac{(m_1 - m_2) \times 100}{m_1} \quad (2)$$

Additionally, the appearance of all metal plates before and after 20 weeks (3360 h) of immersion in the six biodiesel-diesel blends (B0, B25, B50, B75, and B100) are presented in Figures 7–11.

Additionally, the corrosion morphologies of metal surfaces were analyzed using Bresser LCD MICRO 5MP digital microscope images, with 10× magnification, and the surface exposed to biodiesel-diesel blends are displayed in Figures 12–16. The images reveal that after exposure to biodiesel-diesel blends, corrosion caused a slight change in the metal surface.

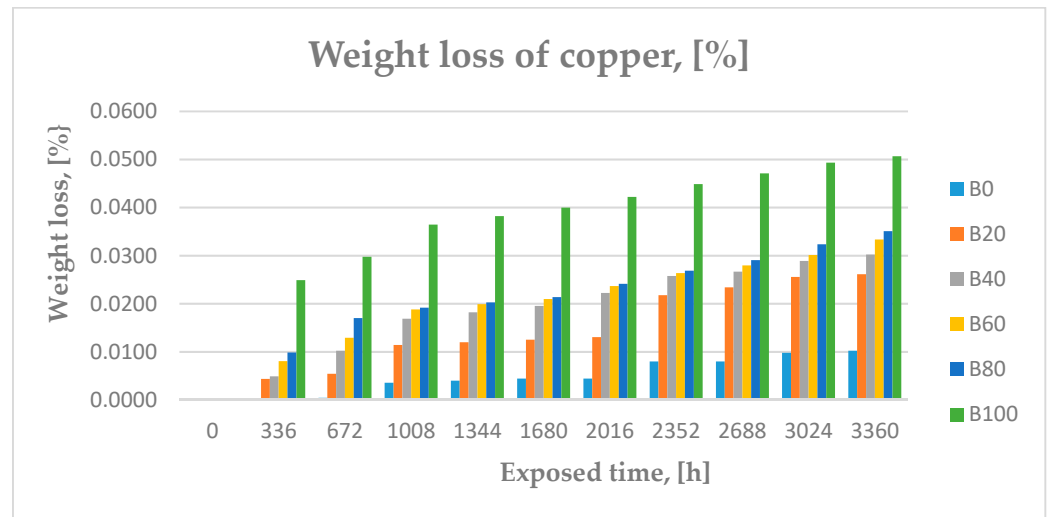


Figure 1. Weight loss of copper plates measured every 336 h for 3360 h, [%].

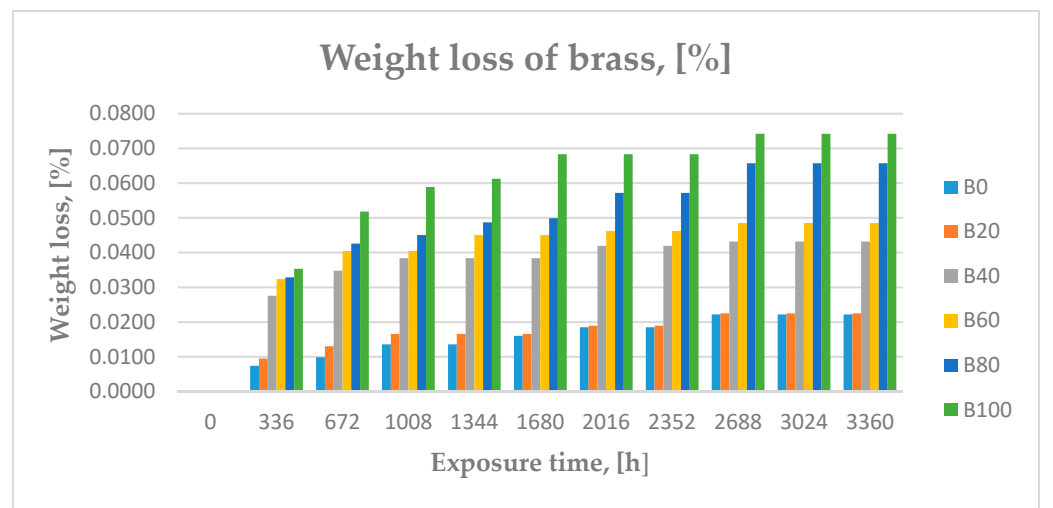


Figure 2. Weight loss of brass plates measured every 336 h for 3360 h, [%].



Figure 3. Weight loss of aluminum plates measured every 336 h for 3360 h, [%].



Figure 4. Weight loss of zinc plates measured every 336 h for 3360 h, [%].



Figure 5. Weight loss of stainless steel plates measured every 336 h for 3360 h, [%].

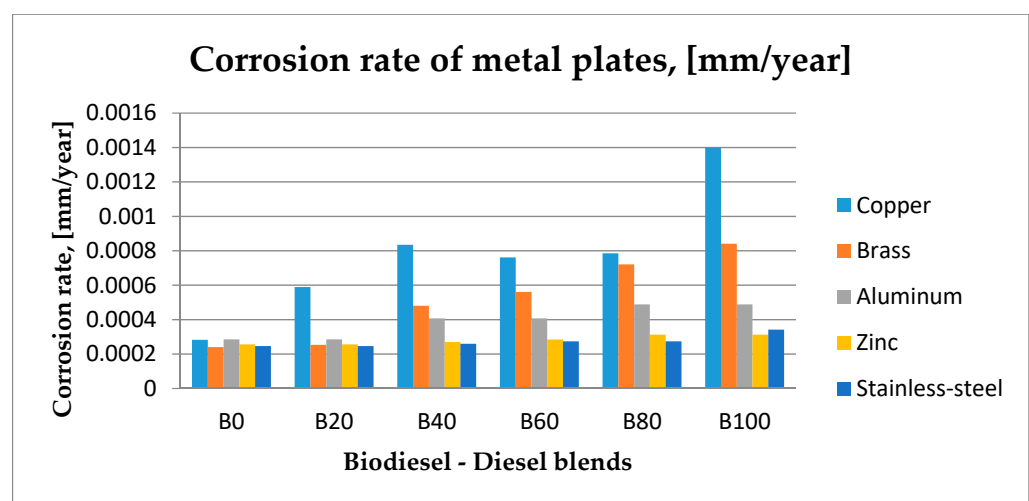


Figure 6. Corrosion rate of copper, brass, aluminum, zinc, and stainless steel after 3360 h of immersion in B0, B20, B40, B60, B80, and B100.

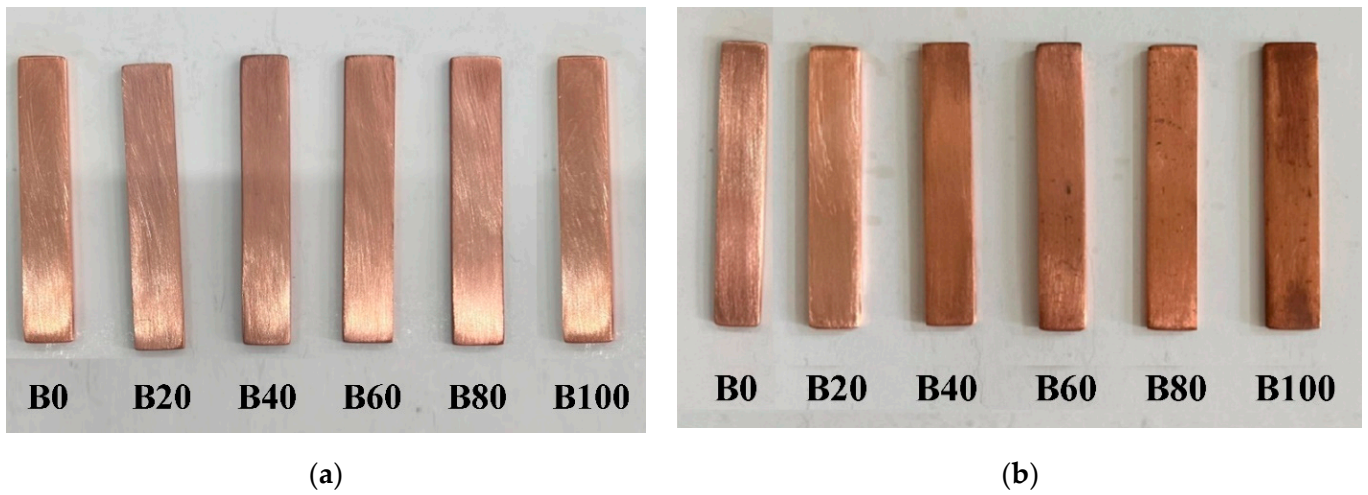


Figure 7. Appearance of the copper plates before (a) and after (b) 20 weeks of immersion in six biodiesel-diesel blends (B0, B20, B40, B60, B80, and B100).

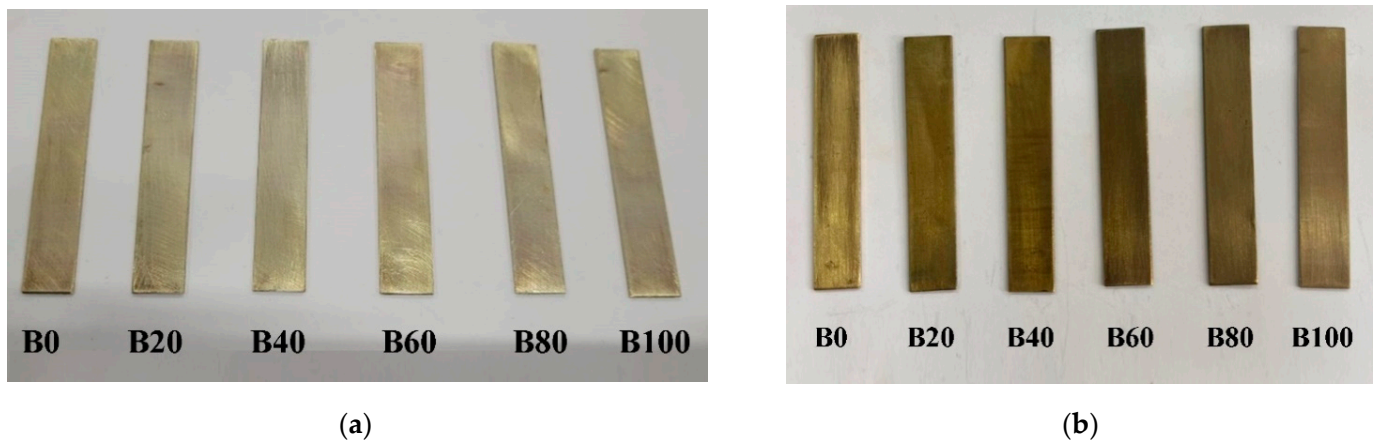


Figure 8. Appearance of the brass plates before (a) and after (b) 20 weeks of immersion in six biodiesel-diesel blends (B0, B20, B40, B60, B80, and B100).

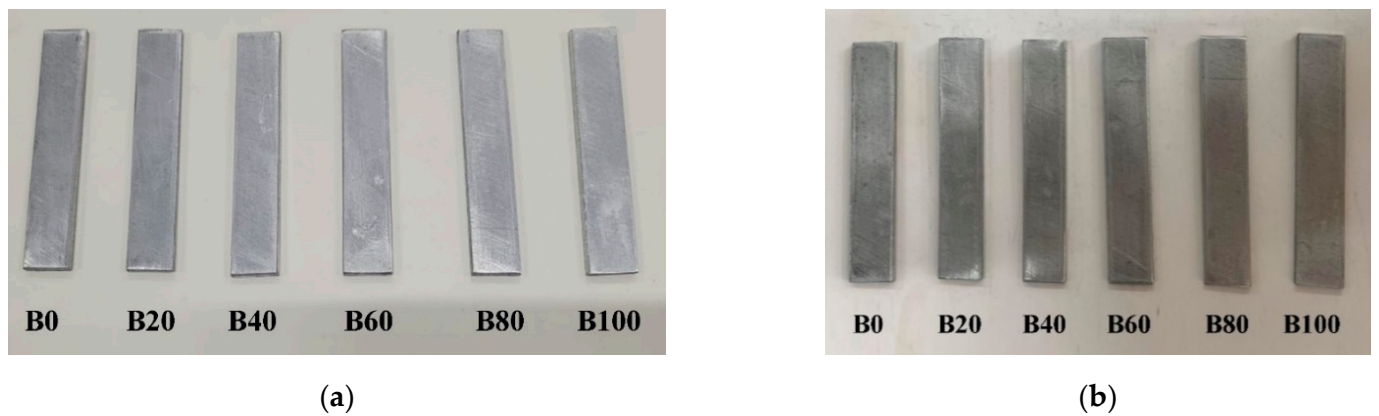
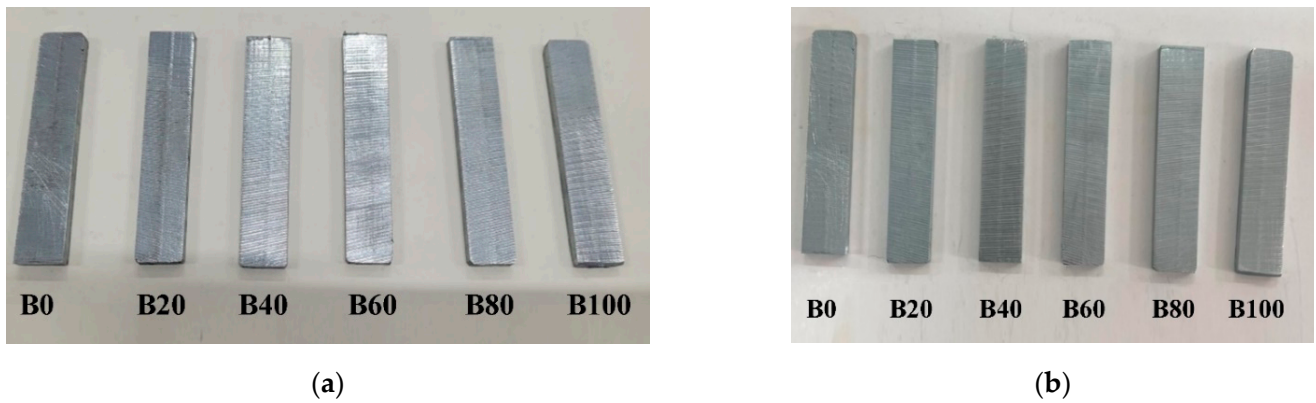


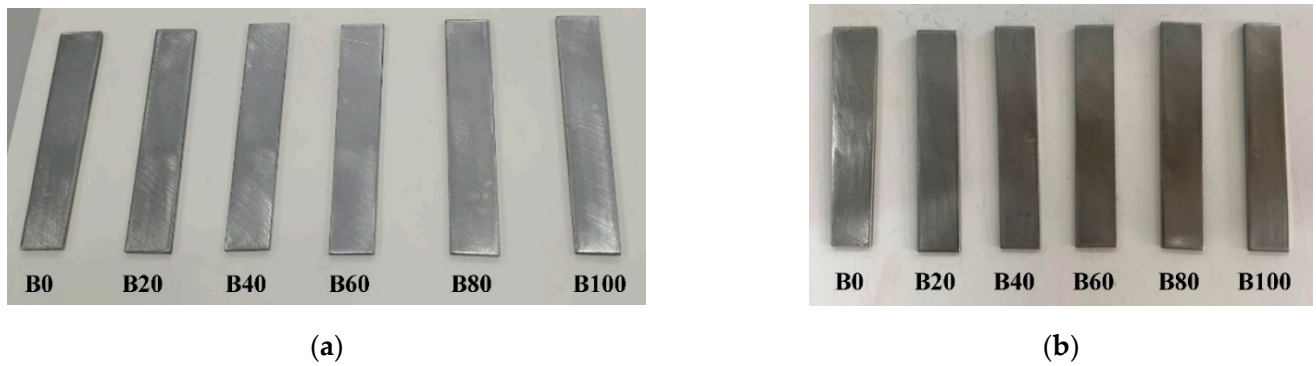
Figure 9. Appearance of the aluminum plates before (a) and after (b) 20 weeks of immersion in six biodiesel-diesel blends (B0, B20, B40, B60, B80, and B100).



(a)

(b)

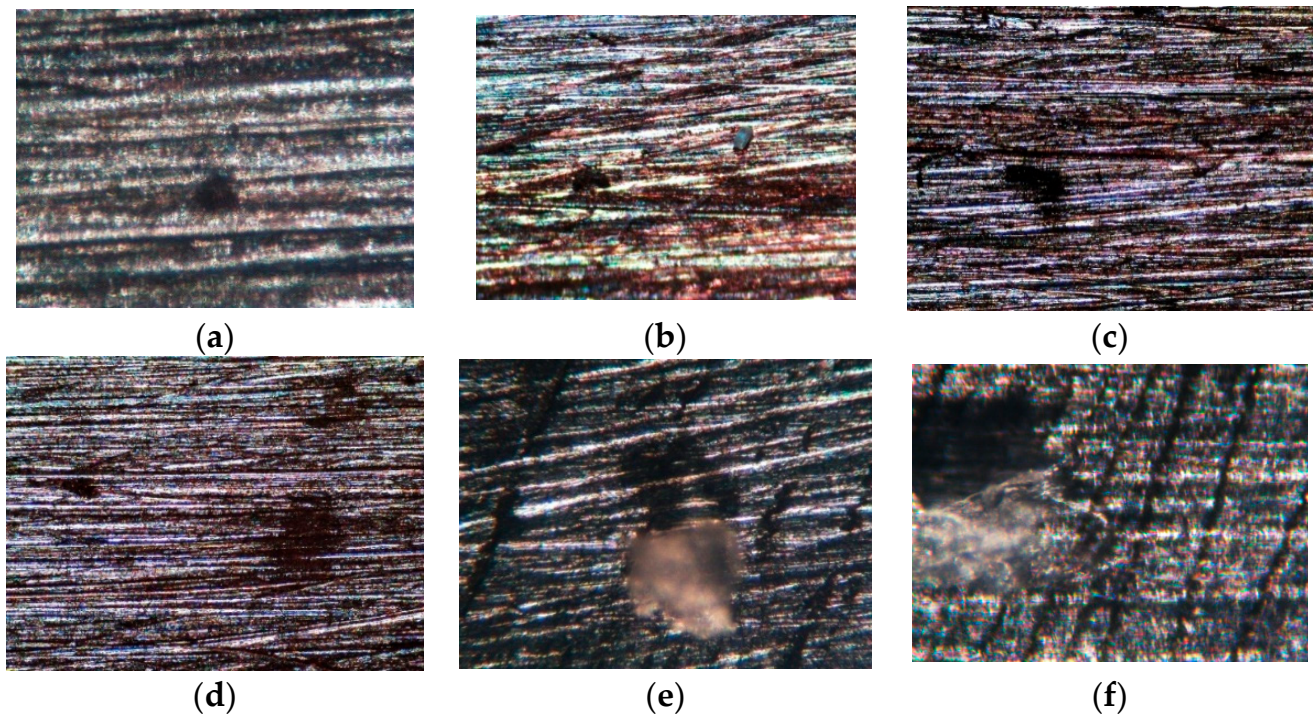
Figure 10. Appearance of the zinc plates before (a) and after (b) 20 weeks of immersion in six biodiesel-diesel blends (B0, B20, B40, B60, B80, and B100).



(a)

(b)

Figure 11. Appearance of the stainless steel plates before (a) and after (b) 20 weeks of immersion in six biodiesel-diesel blends (B0, B20, B40, B60, B80, and B100).



(a)

(b)

(c)

(d)

(e)

(f)

Figure 12. Optical photographs showing the morphological changes of the copper surface after exposure to biodiesel-diesel blends: B0 (a), B20 (b), B40 (c), B60 (d), B80 (e), and B100 (f) at room temperature for 3360 h.

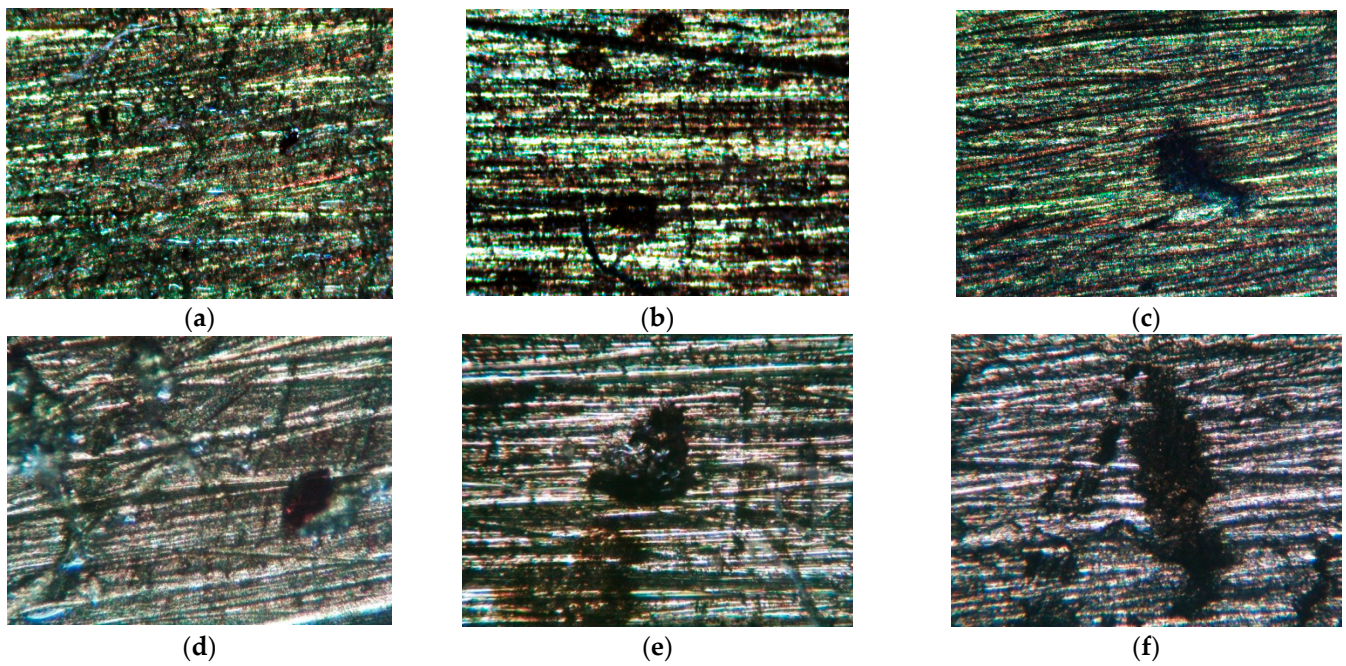


Figure 13. Optical photographs showing the morphological changes of the brass surface after exposure to biodiesel-diesel blends: B0 (a), B20 (b), B40 (c), B60 (d), B80 (e), and B100 (f) at room temperature for 3360 h.

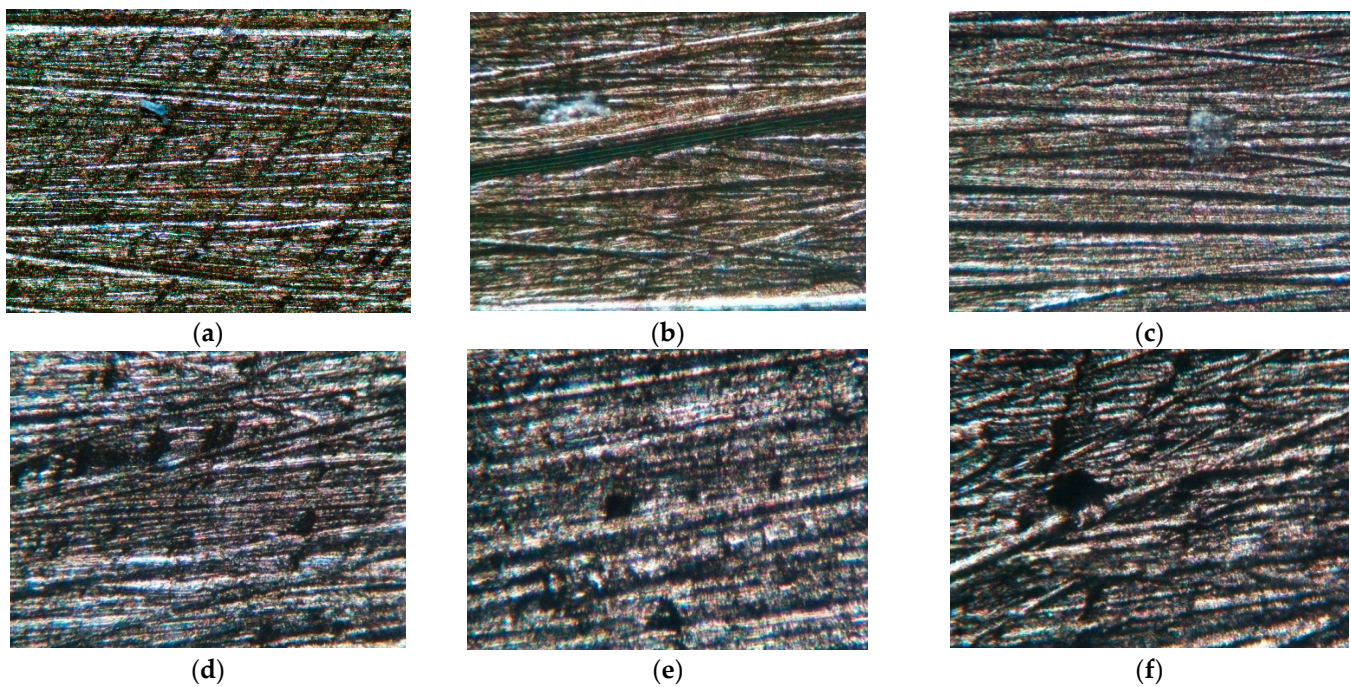


Figure 14. Optical photographs showing the morphological changes of aluminum surface after exposure to biodiesel-diesel blends: B0 (a), B20 (b), B40 (c), B60 (d), B80 (e), and B100 (f) at room temperature for 3360 h.

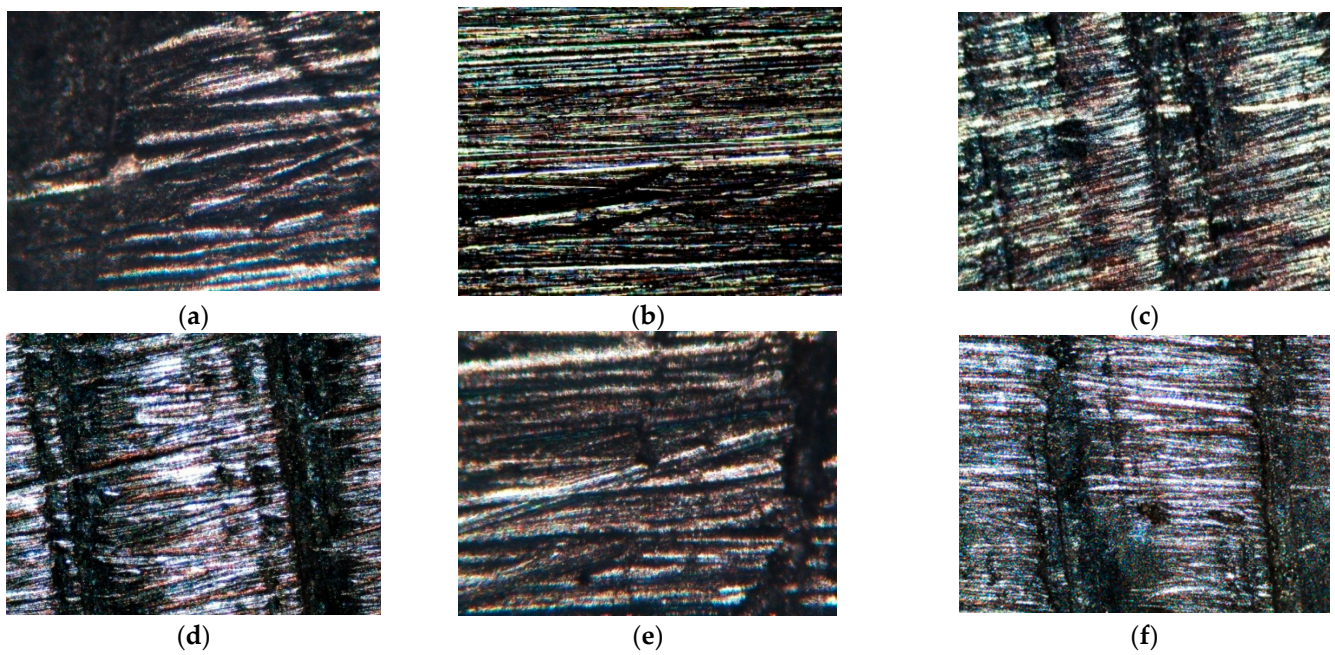


Figure 15. Optical photographs showing the morphological changes of zinc surface after exposure to biodiesel-diesel blends: B0 (a), B20 (b), B40 (c), B60 (d), B80 (e), and B100 (f) at room temperature for 3360 h.

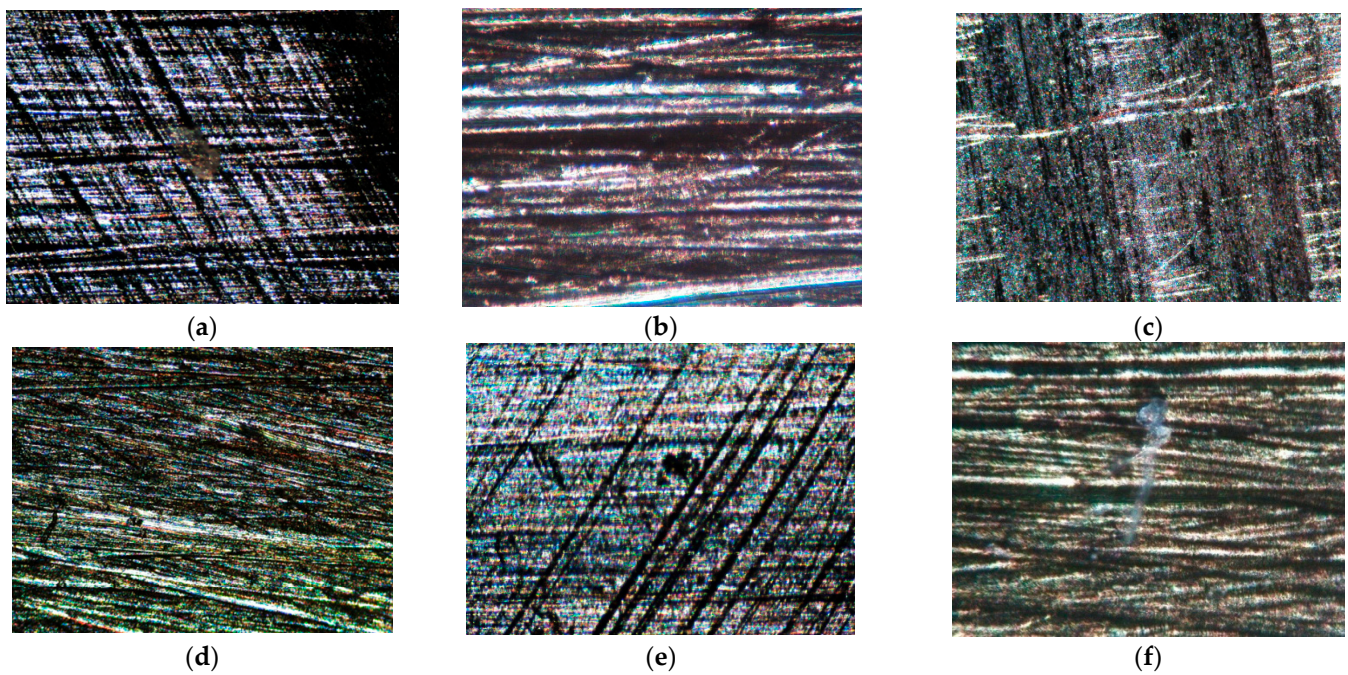


Figure 16. Optical photographs showing the morphological changes of stainless steel surface after exposure to biodiesel-diesel blends: B0 (a), B20 (b), B40 (c), B60 (d), B80 (e), and B100 (f) at room temperature for 3360 h.

The measured total acid numbers of different fuels before and after exposure to metals at room temperature for 3360 h are shown in Table 3.

Table 3. Change in total acid numbers (TAN) of different fuels (B0, B20, B40, B60, B80, and B100) before (as received) and after exposure to metals, at room temperature, for 3360 h.

Total Acid Number (TAN), [mg KOH/g]	B0	B20	B40	B60	B80	B100
As received	0.256	0.265	0.275	0.284	0.291	0.298
Copper	0.258	0.269	0.289	0.301	0.307	0.318
Brass	0.257	0.268	0.286	0.294	0.303	0.316
Aluminum	0.256	0.271	0.278	0.287	0.295	0.299
Zinc	0.257	0.270	0.279	0.287	0.295	0.300
Stainless steel	0.256	0.267	0.278	0.283	0.293	0.299

4. Discussion

4.1. Mass Loss and Changes in Surface Morphology

The corrosion response of metals is a significant consideration when utilizing biodiesel as an engine fuel. These five metals/alloy materials (copper, brass, aluminum, zinc, and stainless steel) were selected for this experiment because components like engine blocks, piston parts, and cylinder heads often utilize aluminum and its alloys in diesel engines. Similarly, copper and its derivatives find application in components such as fuel pumps and injectors. Additionally, stainless steel is typically employed for valve bodies, fuel filters, and pump rings, as noted by Hoang et al. [9]. Furthermore, variables like the composition of biodiesel and environmental conditions play crucial roles in determining the extent and types of corrosion. Notably, copper, aluminum, and steel are frequently chosen materials in diesel engine construction, as highlighted by Nguyen and Vu [55]. The immersion tests were carried out at room temperature, specifically between 20 °C and 25 °C, for a duration of 3360 h. This approach considered both the fuel system of the diesel engine and the storage conditions of fuel blends, which typically occur at normal temperatures in the 20–25 °C range.

The diverse corrosion responses of various metals to biodiesel derived from rapeseed oil and its diesel blends were ascertained by evaluating their percentage weight loss, as depicted in Figures 1–5, and by determining the corrosion rates calculated with Equation (1) and illustrated in Figure 6.

Figures 1–5 indicate that the weight loss of all metal plates increases at higher concentrations of biodiesel in blends. From all analyzed metals, copper and brass present a higher value of weight loss compared to aluminum, zinc, and stainless steel in all biodiesel-diesel blends.

The corruptions of copper and brass were more severe than those of aluminum, zinc, and stainless steel in biodiesel-diesel blends. The corrosion rate of copper in biodiesel was five times faster than that in diesel, and the corrosion rate of brass in biodiesel was 3.5 times faster than that in diesel. The corrosion rate values for copper plates, assessed at room temperature over a span of 3360 h, ranged from 0.0002 mm/year in B0 to 0.0014 mm/year in B100. This is notably lower than the 0.02334 mm/year rate documented by Hu et al. [18] for copper corrosion in B100 derived from rapeseed oil, observed at 43 °C over 1440 h. These findings suggest that as the temperature rises, the corrosion rate tends to increase, even when the exposure duration is reduced.

In contrast, the impact of biodiesel on aluminum, zinc, and stainless steel exhibited minimal corrosion effects, similar to those observed with diesel.

The corrosion rate measurements for stainless steel plates, conducted at room temperature for 3360 h, varied between 0.00024 mm/year in B0 and 0.00034 mm/year in B100. These values are also significantly less than the 0.00087 mm/year rate reported by Hu et al. [18] for copper corrosion in B100 sourced from rapeseed oil, studied at 43 °C for 1440 h. Such results indicate that with increased temperatures, the rate of corrosion typically amplifies, even for a shorter exposure time. These effects of biodiesel on the metals were caused by the oxidation of components in biodiesel, oxygen, and active atom oxygen in biodiesel, leading to the creation of metal oxides [12,56].

Copper and brass were easily oxidized, initiating rapid chemical reactions to form metal oxides. In contrast, aluminum, zinc, and stainless steel facilitated the development of protective metal oxide films, mitigating oxidation and resulting in reduced corrosion rates. These oxide films acted as barriers, preventing both oxygen atoms and the biodiesel sample from interacting directly with the metal surface, thereby minimizing corrosion rates.

Furthermore, all five metals showcased reduced corrosion rates when exposed to diesel. This is attributed to the inherent chemical stability of diesel, characterized by its composition of saturated hydrocarbons.

Observations from optical images in Figures 12–16 reveal heightened corrosion on metal surfaces when immersed in biodiesel compared to diesel after a 3360 h immersion test. Notably, distinct micro pits or dark spots were evident on the metal surfaces, particularly with increased biodiesel concentrations. Copper exhibited a heightened vulnerability to corrosion in biodiesel and its blends compared to aluminum and steel. This behavior may be linked to the enhanced conductivity of copper or its alloys (like brass) relative to iron-based alloys (such as stainless steel) and aluminum-based alloys, as noted by Román et al. [57]. Additionally, the increased corrosion rate of copper and its alloys in biodiesel, relative to other metals, has been corroborated using Open Circuit Potential (OCP) assessments, as highlighted by Rocabrundo-Valdés et al. [58].

4.2. Changes in Biodiesel Properties

The total acid number serves as an indicator of the acidic content present in the fuel, as defined by this particular standard. Based on Table 3, it's evident that biodiesel, when in contact with various metals, exhibited gradual deterioration, as indicated by a rise in the TAN value with an escalating concentration of biodiesel in the blends. However, TAN in all tested metals consistently stayed well below the standard maximum value of 0.5 mg KOH/g. The TAN values for diesel exposed to all analyzed metals closely resemble those of the original diesel. In contrast, biodiesel blends exhibit an increase in TAN values when exposed to metals, with a more pronounced effect in higher blends. This increase in TAN values upon metal exposure is consistent across all metals. It may be noted, however, that the extent of corrosion is greater for copper and brass than for aluminum, zinc, and stainless steel. An elevated TAN number signifies fuel oxidation [59]. A comparison of TAN values for fuel exposed to copper and brass indicates faster corrosion with copper, suggesting intrinsic weakness in copper within biodiesel-diesel blends compared to brass. The presence of alloying elements, such as zinc, is believed to contribute to enhanced corrosion resistance. Consequently, we can assert that if a fuel meets the necessary oxidation stability requirements, storage stability of at least 140 days can be guaranteed under typical storage conditions.

5. Conclusions

The effect of biodiesel-diesel blends B0, B20, B40, B60, B80, and B100 on different metals/alloys such as copper, brass, aluminum, zinc, and stainless steel was investigated using static immersion test at room temperature for 3360 h. The following points have been concluded from this study:

1. Copper and brass are susceptible to corrosion in biodiesel-diesel blends, whereas aluminum, zinc, and stainless steel exhibit high corrosion resistance.
2. The corrosion rate of copper and brass in biodiesel was, 5 and 3.5 times faster than that in diesel fuel, respectively. On the other side, the corrosion effects of biodiesel on aluminum, zinc, and stainless steel were minor, close to those of diesel.
3. After 3360 h of immersion test, pitting corrosion was observed from optical photographs of metal surfaces, especially on higher biodiesel concentrations.
4. Samples with lower biodiesel content exhibited a moderate decrease in resistance to degradation.

5. With higher biodiesel content, degradation, as indicated by the TAN, became more pronounced, yet even in these circumstances, the maximum values were below the standard of 0.5 mg KOH/g.

Studying the corrosion effect of a biodiesel-diesel blend on different metals/alloys used as automotive components can have several practical applications. Here, are some potential applications based on the experimental work:

- The findings can guide automotive manufacturers in selecting appropriate materials for components that come into contact with biodiesel-diesel blends. For instance, if certain alloys are found to resist corrosion better than others, they can be preferred for specific applications.
- The research can aid in optimizing biodiesel-diesel blend formulations to minimize corrosion. By understanding which metals/alloys are more susceptible to corrosion, fuel producers can adjust the blend composition or introduce additives to reduce corrosive effects.

Moving forward, we plan to extend our research on the corrosion characteristics of various metals/alloys within biodiesel-diesel blends, focusing on elevated temperatures and conditions relevant to operational engine settings.

Author Contributions: Conceptualization, A.E.S. and O.V.S.; methodology, A.E.S. and B.G.S.; software, T.V.C.; validation, A.E.S. and O.V.S.; investigation, B.G.S. and T.V.C.; writing—original draft preparation, O.V.S. and A.E.S.; writing—review and editing, A.E.S. and O.V.S.; supervision, A.E.S. All authors have read and agreed to the published version of the manuscript.

Funding: This research received no external funding.

Data Availability Statement: All data used to support this study are included within the article.

Conflicts of Interest: The authors declare no conflicts of interest.

References

1. Aghbashlo, M.; Tabatabaei, M.; Mohammadi, P.; Khoshnevisan, B.; Rajaeifar, M.A.; Pakzad, M. Neat diesel beats waste-oriented biodiesel from the exergoeconomic and exergoenvironmental point of views. *Energy Convers. Manag.* **2017**, *148*, 1–15. [CrossRef]
2. Hosseinzadeh-Bandbafha, H.; Tabatabaei, M.; Aghbashlo, M.; Khanali, M.; Demirbas, A. A comprehensive review on the environmental impacts of diesel/biodiesel additives. *Energy Convers. Manag.* **2018**, *174*, 579–614. [CrossRef]
3. Takase, M.; Pappoe, A.N.M.; Afrifa, E.A.; Miyittah, M. High performance heterogeneous catalyst for biodiesel production from non-edible oil. *Renew. Energy Focus* **2018**, *25*, 24–30. [CrossRef]
4. Aghbashlo, M.; Tabatabaei, M.; Khalife, E.; Roodbar Shojaei, T.; Dadak, A. Exergoeconomic analysis of a DI diesel engine fueled with diesel/biodiesel (B5) emulsions containing aqueous nano cerium oxide. *Energy* **2018**, *149*, 967–978. [CrossRef]
5. Hoang, A.T.; Pham, V.V. A study of emission characteristic, deposits, and lubrication oil degradation of a diesel engine running on preheated vegetable oil and diesel oil. *Energy Sources Part A Recovery Util. Environ. Eff.* **2019**, *41*, 611–625. [CrossRef]
6. Hoang, A.T.; Pham, V.V. Impact of jatropha oil on engine performance, emission characteristics, deposit formation, and lubricating oil degradation. *Combust. Sci. Technol.* **2019**, *191*, 504–519. [CrossRef]
7. Chandran, D.; Ng, H.K.; Lau, H.L.N.; Gan, S.; Choo, Y.M. Investigation of the effects of palm biodiesel dissolved oxygen and conductivity on metal corrosion and elastomer degradation under novel immersion method. *Appl. Therm. Eng.* **2016**, *104*, 294–308. [CrossRef]
8. Yeşilyurt, M.K.; Öner, İ.V.; Yilmaz, E.Ç. Biodiesel Induced Corrosion and Degradation: A Review. *Pamukkale Üniv. Mühendislik Bilim. Derg.* **2019**, *25*, 60–70. [CrossRef]
9. Hoang, A.T.; Tabatabaei, M.; Aghbashlo, M. A review of the effect of biodiesel on the corrosion behavior of metals/alloys in diesel engines. *Energy Sources Part A Recovery Util. Environ. Eff.* **2020**, *42*, 2923–2943. [CrossRef]
10. Fraer, R.; Dinh, H.; Proc, K.; McCromick, R.L.; Chandler, K.; Buchholz, B. *Operating Experience and Teardown Analysis for Engines Operated on Biodiesel Blends (B20)*; SAE International 2005-01-3641; Rosemont, IL, USA, 2005; p. NREL/CP-540-38509. Available online: <https://www.sae.org/publications/technical-papers/content/2005-01-3641/> (accessed on 14 December 2023).
11. DOE/GO-102006-2356; Biodiesel Handling and Guidelines. 3rd ed. Department of Energy: Washington, DC, USA, 2006.
12. Haseeb, A.S.M.A.; Masjuki, H.H.; Ann, L.J.; Fazal, M.A. Corrosion characteristics of copper and leaded bronze in palm biodiesel. *Fuel Process. Technol.* **2010**, *91*, 329–334. [CrossRef]
13. Ahmmad, M.S.; Hassan, H.; Bin, M.; Kalam, M.A. Comparative corrosion characteristics of automotive materials in Jatropha biodiesel. *Int. J. Green Energy* **2018**, *15*, 393–399. [CrossRef]
14. Thangavelu, S.K.; Ahmed, A.S.; Ani, F.N. Impact of metals on corrosive behavior of biodiesel–Diesel–Ethanol (BDE) alternative fuel. *Renew. Energy* **2016**, *94 Pt C*, 1–9. [CrossRef]

15. Sgroi, M.; Bollito, G.; Saracco, G.; Specchia, S. BIOFEAT: Biodiesel fuel processor for a vehicle fuel cell auxiliary power unit: Study of the feed system. *J. Power Sources* **2005**, *149*, 8–14. [[CrossRef](#)]
16. Fazal, M.A.; Haseeb, A.S.M.A.; Masjuki, H.H. Effect of temperature on the corrosion behavior of mild steel upon exposure to palm biodiesel. *Energy* **2011**, *35*, 3328–3334. [[CrossRef](#)]
17. Baena, L.M.; Calderón, J.A. Effects of palm biodiesel and blends of biodiesel with organic acids on metals. *Heliyon* **2020**, *6*, e03735. [[CrossRef](#)] [[PubMed](#)]
18. Hu, E.; Xu, Y.; Hu, X.; Pan, L.; Jiang, S. Corrosion behaviors of metals in biodiesel from rapeseed oil and methanol. *Renew. Energy* **2012**, *37*, 371–378. [[CrossRef](#)]
19. Geller, D.P.; Adams, T.T.; Goodrum, J.W.; Pendergrass, J. Storage stability of poultry fat and diesel fuel mixtures: Part II—Chemical properties. *Fuel* **2010**, *89*, 792–796. [[CrossRef](#)]
20. Aquino, I.P.; Hernandez, R.P.B.; Chicoma, D.L.; Pinto, H.P.F.; Aoki, I.V. Influence of light, temperature and metallic ions on biodiesel degradation and corrosiveness to copper and brass. *Fuel* **2012**, *102*, 795–807. [[CrossRef](#)]
21. Fazal, M.A.; Suhaila, N.R.; Haseeb, A.S.M.A.; Rubaiee, S. Sustainability of additive-doped biodiesel: Analysis of its aggressiveness toward metal corrosion. *J. Clean. Prod.* **2018**, *181*, 508–516. [[CrossRef](#)]
22. Kugelmeier, C.L.; Monteiro, M.R.; da Silva, R.; Kuri, S.E.; Sordi, V.L.; Della Rovere, C.A. Corrosion behavior of carbon steel, stainless steel, aluminum and copper upon exposure to biodiesel blended with petrodiesel. *Energy* **2021**, *226*, 120344. [[CrossRef](#)]
23. Thangarasu, V.; Balaji, B.; Ramanathan, A. Experimental investigation of tribo-corrosion and engine characteristics of Aegle Marmelos Correa biodiesel and its diesel blends on direct injection diesel engine. *Energy* **2019**, *171*, 879–892. [[CrossRef](#)]
24. Sterpu, A.E.; Dumitru, A.I.; Popa, M.F. Corrosion behavior of steel in biodiesel of different origin. *Ovidius Univ. Ann. Chem.* **2012**, *23*, 143–148. [[CrossRef](#)]
25. Decote, P.A.P.; Negriz, L.; Vidoto, A.P.; Mendes, L.A.N.; Flores, E.M.M.; Vicente, M.A.; Santos, M.F.P. Determination of the total acid number of Brazilian crude oil samples: Theoretical and experimental evaluation of three standard methods. *Fuel* **2022**, *313*, 122642. [[CrossRef](#)]
26. Wang, H.; Tang, H.; Wilson, J.; Salley, S.O.; Ng, S. Total Acid Number Determination of Biodiesel and Biodiesel Blends. *J. Am. Oil Chem. Soc.* **2008**, *85*, 1083–1086. [[CrossRef](#)]
27. SR EN 14103. Standard Test Method for Determination of Ester and Linolenic Acid Methyl Ester Contents in Fatty Acid Methyl Esters (FAME). Available online: <https://standards.iteh.ai/catalog/standards/cen/2eb3696f-7f13-49f2-846e-0ebd8f4c42ea/en-14103-2020> (accessed on 14 December 2023).
28. SR EN 16300. Standard Test Method for Determination of Iodine Value in Fatty Acid Methyl Esters (FAME). Available online: <https://cdn.standards.iteh.ai/samples/35004/c156163013804b67a2331c72f24562ac/SIST-EN-16300-2012.pdf> (accessed on 14 December 2023).
29. SR EN ISO 12185. Standard Test Methods for Crude Oils and Petroleum Products—Determination of Density—Oscillating U-tube Method. Available online: <https://cdn.standards.iteh.ai/samples/367/9c903f5ef3284d23a5cfb5412b91506e/SIST-EN-ISO-12185-1998.pdf> (accessed on 14 December 2023).
30. SR EN ISO 3104. Standard Test Methods for Petroleum Products—Transparent and Opaque Liquids—Determination of Kinematic Viscosity and Calculation of Dynamic Viscosity. Available online: <https://cdn.standards.iteh.ai/samples/67965/c8a7502f7eed44eab5c798eae73fe41/ISO-3104-2020.pdf> (accessed on 14 December 2023).
31. SR EN ISO 12937. Standard Test Methods for Determination of Water—Coulometric Karl Fischer Titration Method. Available online: <https://cdn.standards.iteh.ai/samples/2730/d1f8ee11083a4fbc84aad409e4bcf40f/ISO-12937-2000.pdf> (accessed on 14 December 2023).
32. SR EN 14110. Standard Test Methods for Fat and Oil Derivatives—Fatty Acid Methyl Esters—Determination of Methanol Content. Available online: <https://cdn.standards.iteh.ai/samples/64247/3cb8686024644c7bb52f45eab89d5e0b/SIST-EN-14110-2019.pdf> (accessed on 14 December 2023).
33. SR EN ISO 3679. Standard Test Methods for Determination of Pass-No-Pass Flammability and Flash Point. Fast Closed-Vessel Equilibrium Method. Available online: <https://cdn.standards.iteh.ai/samples/29076/342956b390f44d48a60f739b6cd14bb3/ISO-3679-2004.pdf> (accessed on 14 December 2023).
34. SR EN ISO 20884. Standard Test Methods for Petroleum products—Determination of Sulfur Content of Automotive Fuels—Wavelength-Dispersive X-ray Fluorescence Spectrometry. Available online: <https://standards.iteh.ai/catalog/standards/cen/2156a459-967a-46dc-9f39-84ec125456ba/en-iso-20884-2019> (accessed on 14 December 2023).
35. SR EN 14112. Standard Test Methods for Fat and Oil Derivatives—Fatty Acid Methyl Esters (FAME)—Determination of Oxidation Stability (Accelerated Oxidation Test). Available online: <https://cdn.standards.iteh.ai/samples/66922/49757a201d91465c837f02ac2541337d/SIST-EN-14112-2021.pdf> (accessed on 14 December 2023).
36. SR EN 14104. Standard Test Methods for Fat and Oil Derivates. Fatty Acid Methyl Ester (FAME). Determination of Acid Value. Available online: <https://cdn.standards.iteh.ai/samples/70045/1a81e80332be42e299fa8d3f5cdc20f2/SIST-EN-14104-2021.pdf> (accessed on 14 December 2023).
37. SR EN 14105. Standard Test Methods for Fat and Oil Derivatives. Fatty Acid Methyl Esters (FAME). Determination of Free and Total Glycerol and Mono-, di-, Triglyceride Contents. Available online: <https://cdn.standards.iteh.ai/samples/66921/3bcfc94d6a8248a484e874ea42d649df/SIST-EN-14105-2021.pdf> (accessed on 14 December 2023).

38. SR EN 116/AC. Standard Test Methods for Diesel Engine Fuels. Determination of Cold Filter Plugging Point. Available online: <https://standards.iteh.ai/catalog/standards/cen/f0b4bc72-e8b9-4969-b957-8e6ce72f489d/en-116-2015> (accessed on 14 December 2023).
39. SR EN 23015. Standard Test Methods for Petroleum Products—Determination of Cloud Point. Available online: <https://standards.iteh.ai/catalog/standards/cen/616161ad-c21a-4355-8482-0a4f1dae8a47/en-23015-1994> (accessed on 14 December 2023).
40. SR EN 12662. Standard Test Methods for Liquid Petroleum Products—Determination of Total Contamination in Middle Distillates, Diesel Fuels and Fatty acid Methyl Esters. Available online: <https://cdn.standards.iteh.ai/samples/33063/6ce689c2e25c487c94728b343aca06eb/SIST-EN-12662-2014.pdf> (accessed on 14 December 2023).
41. ASTM D 4052-22. Standard Test Method for Density, Relative Density, and API Gravity of Liquids by Digital Density Meter. Available online: <https://cdn.standards.iteh.ai/samples/112378/1e427858c52b4fff89a470b85eeda29d/ASTM-D4052-22.pdf> (accessed on 14 December 2023).
42. ASTM D 1500-12. Standard Test Method for ASTM Color of Petroleum Products (ASTM Color Scale). Available online: <https://cdn.standards.iteh.ai/samples/83766/6e4dbd875aee4069b0729429ba8387f1/ASTM-D1500-12.pdf> (accessed on 14 December 2023).
43. ASTM D 93-20. Standard Test Methods for Flash Point by Pensky-Martens Closed Cup Tester. Available online: <https://cdn.standards.iteh.ai/samples/106978/1302886874ea49afb428f047cc06313a/ASTM-D93-20.pdf> (accessed on 14 December 2023).
44. SR EN ISO 20846. Standard Test Methods for Petroleum products—Determination of Sulfur Content of Automotive Fuels—Ultraviolet Fluorescence Method. Available online: <https://cdn.standards.iteh.ai/samples/74313/a425278694264f5e83a5583af8f65cf2/ISO-20846-2019.pdf> (accessed on 14 December 2023).
45. SR EN ISO 2160. Standard Test Methods for Petroleum Products. Corrosiveness to Copper. Copper Strip Test. Available online: <https://cdn.standards.iteh.ai/samples/6951/bf3676429b7d4e3182795258b7e281e5/ISO-2160-1985.pdf> (accessed on 14 December 2023).
46. SR EN ISO 10370. Standard Test Methods for Petroleum Products—Determination of Carbon Residue—Micro Method. Available online: <https://cdn.standards.iteh.ai/samples/57081/58db305ae9c5498db6ecb951674cf4e0/ISO-10370-2014.pdf> (accessed on 14 December 2023).
47. SR EN ISO 6245. Standard Test Methods for Petroleum Products. Determination of Ash. Available online: <https://cdn.standards.iteh.ai/samples/31156/247005c940e042f7a79ff4e0c5d6edba/ISO-6245-2001.pdf> (accessed on 14 December 2023).
48. SR EN ISO 4264. Standard Test Methods for Petroleum Products—Calculation of Cetane Index of Middle-Distillate Fuels by the four Variable Equation. Available online: <https://cdn.standards.iteh.ai/samples/45627/c254c9d0f08545ce9abc39ea6d1eb404/ISO-4264-2007.pdf> (accessed on 14 December 2023).
49. ASTM D 2500-17a. Standard Test Method for Cloud Point of Petroleum Products and Liquid Fuels. Available online: <https://cdn.standards.iteh.ai/samples/99033/1f30ba3334a04c668e23c632698ab322/ASTM-D2500-17a.pdf> (accessed on 14 December 2023).
50. ASTM D 6371-17a. Standard Test Method for Cold Filter Plugging Point of Diesel and Heating Fuels. Available online: <https://cdn.standards.iteh.ai/samples/97393/c8ce7f68eaa742ffbc5e060dac8df13/ASTM-D6371-17.pdf> (accessed on 14 December 2023).
51. ASTM E 203-16. Standard Test Method for Water Using Volumetric Karl Fischer Titration. Available online: <https://cdn.standards.iteh.ai/samples/94281/136a27289f5444cf837cf8e242aa84f0/ASTM-E203-16.pdf> (accessed on 14 December 2023).
52. SR EN ISO 3405. Standard Test Method for Petroleum and Related Products from Natural or Synthetic Sources—Determination of Distillation Characteristics at Atmospheric Pressure. Available online: <https://cdn.standards.iteh.ai/samples/67956/379a350656fd40f2b3e2f0d5a12e8751/ISO-3405-2019.pdf> (accessed on 14 December 2023).
53. SR EN 14078. Standard Test Method for Liquid Petroleum Products—Determination of Fatty Acid Methyl Ester (FAME) Content in Middle Distillates. Infrared Spectrometry Method. Available online: <https://standards.iteh.ai/catalog/standards/cen/2bc7edd-f6da-43f0-818c-e7ecafe87907/en-14078-2014> (accessed on 14 December 2023).
54. ASTM D 1250. 19e1-Standard Guide for the Use of the Joint API and ASTM Adjunct for Temperature and Pressure Volume Correction Factors for Generalized Crude Oils, Refined Products, and Lubricating Oils: API MPMS Chapter 11.1. Available online: <https://cdn.standards.iteh.ai/samples/106185/269487f113384090a0024462ba429b4c/ASTM-D1250-19e1.pdf> (accessed on 14 December 2023).
55. Nguyen, X.P.; Vu, H.N. Corrosion of the Metal Parts of Diesel Engines in Biodiesel-Based Fuels. *Int. J. Renew. Energy Dev.* **2019**, *8*, 119–132. [CrossRef]
56. Liu, J.; Fang, Y.K. The dissolved oxygen on the corrosion of 20R steel by biodiesel. *Corros. Protet.* **2009**, *30*, 711–713. (In Chinese)
57. Román, A.S.; Barrientos, M.S.; Noceras, M.Á.; Méndez, C.M.; Ares, A.E. Resistance to corrosion of Al-Cu alloy in biodiesel. *Matéria* **2018**, *23*, e12052.
58. Rocabrundo-Valdés, C.I.; Hernández, J.A.; Juantorena, A.U.; Arenas, E.G.; Lopez-Sesenes, R.; Salinas-Bravo, V.M.; González-Rodríguez, J.G. An electrochemical study of the corrosion behavior of metals in canola biodiesel. *Corros. Eng. Sci. Technol.* **2018**, *53*, 153–162. [CrossRef]
59. Zhou, Y.; Zhang, Z.; Zhao, H.; Zhang, X.; Hu, Z.; Wu, Z.; Li, L. A study on the effects of biodiesels on the properties of elastomers, metals and plastics in diesel fuel system. *Auto. Eng.* **2008**, *30*, 875–879. (In Chinese)

Disclaimer/Publisher’s Note: The statements, opinions and data contained in all publications are solely those of the individual author(s) and contributor(s) and not of MDPI and/or the editor(s). MDPI and/or the editor(s) disclaim responsibility for any injury to people or property resulting from any ideas, methods, instructions or products referred to in the content.